Production of Ultrafine Metal Oxide Aerosol Particles by Thermal Decomposition of Metal Alkoxide Vapors

Ultrafine spherical titanium, silicon, and aluminium oxide particles were prepared by the thermal decomposition of their alkoxide vapors, produced by evaporation and subsequent heating. High-concentration ultrafine particles having geometric mean diameters ranging between 0.01 and 0.06 μm and a geometric standard deviation of about 1.4 were obtained by varying the temperatures of the evaporator containing the liquid alkoxides and the reactor furnace, and the flow rate of carrier gas. For furnace temperatures lower than 400°C for TiO_2 and 1000°C for SiO_2 and Al_2O_3, the particles obtained were found to be amorphous. The observed changes in the particle size distributions due to changes in operating conditions were compared with those predicted theoretically by solving the discrete-continuous aerosol general dynamic equation accounting for coagulation and generation of monomer by thermal decomposition. The effect of monomer number concentration on the size distribution of generated particles was found to be qualitatively explained.

Kikuo Okuyama, Yasuo Kousaka
Noboru Tohge, Satoru Yamamoto
Department of Chemical Engineering
University of Osaka Prefecture
Sakai 591, Japan

Jin Jwang Wu, R. C. Flagan
and J. H. Seinfeld
Department of Chemical Engineering
California Institute of Technology
Pasadena, CA 91125

Introduction

Ultrafine particles of diameters less than 0.1 μm are of interest because they offer excellent possibilities in the production of powder catalysts, ceramics, electronic devices, and many other items. Ultrafine particles have different microscopic physical properties from those of bulk material, because the number of atoms or molecules on the particle surface becomes comparable to that inside the particle. As a result, in ultrafine particles melting points decrease, light absorption increases, and electromagnetic and other properties change, compared with their bulk material counterparts.

At the present time, considerable effort is being expended to produce ultrafine particles of metals, metal oxides, and other metallic compounds. In most current processes particles are produced by liquid phase chemical reaction. Gas phase production of ultrafine particles is currently limited to a few situations, for example carbon black. However, on the laboratory scale, solid aerosol particles have been prepared by a variety of processes involving reactions of vapor molecules to produce a condensable product.

Metal oxide particles have been generated by thermal degradation of metal vapors, e.g., synthesis of metallic oxide particles by chemical reactions of their metal chloride vapors. Matijevic and his coworkers have prepared TiO_2 particles (Vica and Matijevic, 1979) and Al_2O_3 particles (Ingerbrethesen and Matijevic, 1980; Ingerbrethesen et al., 1983) with modal diameters ranging between 0.2 and 0.3 μm by condensing titanium and aluminium alkoxide vapors onto ultrafine AgCl particles. Metal oxide particles were then obtained by hydrolysis of these droplets. Komiyama et al. (1984) and Kanai et al. (1985) prepared titanium oxide particles having diameters between 0.2 and 0.4 μm by thermal decomposition of titanium tetraisopropoxide. The advantage of using alkoxide liquids is that metal oxide particles having amorphous or crystalline structure can be produced at a relatively low temperature. Production of ultrafine metal oxide particles having diameters smaller than 0.1 μm has not been previously reported.

In this work, the production of ultrafine particles of titanium oxide, aluminium oxide, and silicon oxide by the thermal decom-

Correspondence concerning this paper should be addressed to K. Okuyama.

position of their alkoxide vapors has been studied experimentally. The size and number concentration of the ultrafine metallic oxide particles produced are measured by the size-analyzing method recently developed by Kousaka et al. (1985a). The particle size distributions are measured by means of a differential mobility analyzer combined with a condensation nucleus counter, and the particle number concentrations are counted independently by an ultramicroscopic system after enlarging their size in a particle size magnifier. Particles are also collected by using an electrostatic precipitator in order to analyze their shape, crystal structure, and chemical composition by electron microscopy, X-ray diffraction, and infrared spectrophotometry. Experimental results on particle size and number concentration of the particles produced have been compared with the solution of the discrete-continuous general dynamic equation for aerosols accounting for Brownian coagulation and monomer generation by chemical reaction.

Particle Generation System

Figure 1 shows a schematic diagram of the particle generation system used in this study. The system consists of a drying column, a vaporizer, a tubular furnace, a particle size magnifier (PSM), a differential mobility analyzer (DMA) and a mixing type condensation nucleus counter (CNC). Since the alkoxide vapor reacts sensitively with water vapor or oxygen gas, nitrogen gas was passed through the drying column (containing silica gel, calcium sulfate, and magnesium perchlorate) and the deoxidizer (containing powder of activated copper) to obtain a dry carrier gas. The metal alkoxide liquids—titanium tetraisopropoxide (TTIP), $Ti(OC_3H_7)_4$; silicon tetraethoxide (STE), $Si(OC_2H_5)_4$; and aluminum tri-sec-butoxide (ATSB), $Al(OC_4H_9)_3$—were maintained in a heated glass container that served as the vapor source. The laboratory nitrogen supply was regulated by a pressure regulator, cleaned by filters, and metered and delivered to the evaporator. Nitrogen gas having a higher temperature (about 30 to 40°C) than that of the vapor is added to avoid condensation loss of the metal alkoxide vapor before entering the reactor furnace.

Table 1 gives the physical properties of the three alkoxides used in the experiment. Judging from the vapor pressures of the alkoxides, the temperature of evaporator were maintained at 40°C for TTIP, 100°C for ATSB, and 0°C for STE.

The alkoxide vapors thus obtained were continuously introduced into the high-temperature furnace of 30 cm length and 13 mm dia. at flow rates ranging from 0.3 to 4 L/min. This furnace was thermostated with a voltage-regulated heating tape, and its temperature was maintained between 400 and 900°C. Figure 2 shows the general physics of the gas-to-particle conversion process that is expected to occur in the furnace. The metal alkoxide vapor is thermally decomposed to produce supersaturated metal oxide vapor. If this supersaturation of metal oxide vapor reaches a sufficient level, ultrafine primary metal oxide clusters are produced by homogeneous nucleation. Larger secondary particles are formed by the agglomeration of clusters and by the simultaneous heterogeneous condensation of vapor molecule on clusters.

The thermal decomposition of titanium, silicon, and aluminium alkoxide vapors takes place in the furnace according to the following reactions,

$$Ti(OC_3H_7)_4 \rightarrow TiO_2 + 4C_3H_6 + 2H_2O$$
$$Si(OC_2H_5)_4 \rightarrow SiO_2 + 4C_2H_4 + 2H_2O$$
$$2Al(OC_4H_9)_3 \rightarrow Al_2O_3 + 6C_4H_8 + 3H_2O \qquad (1)$$

As seen from the above reactions, the thermal decomposition will produce water vapor and gaseous ethylene, propylene, and butylene, respectively, with the gaseous metal oxide. Measurement of the concentrations of ethylene, propylene, and butylene allows the reaction rates to be determined quantitatively. In the case of the formation of titanium oxide particles, Komiyama et al. (1984) and Kanai et al. (1985) suggested that the thermal decomposition rate of TTIP was approximated by the 0.5-order reaction and that the particle formation was catalyzed by the TiO_2 deposit on the reactor wall. However, the detailed reaction mechanism of Eq. 1 has not been clear until now.

The analysis of particle size and number concentration of

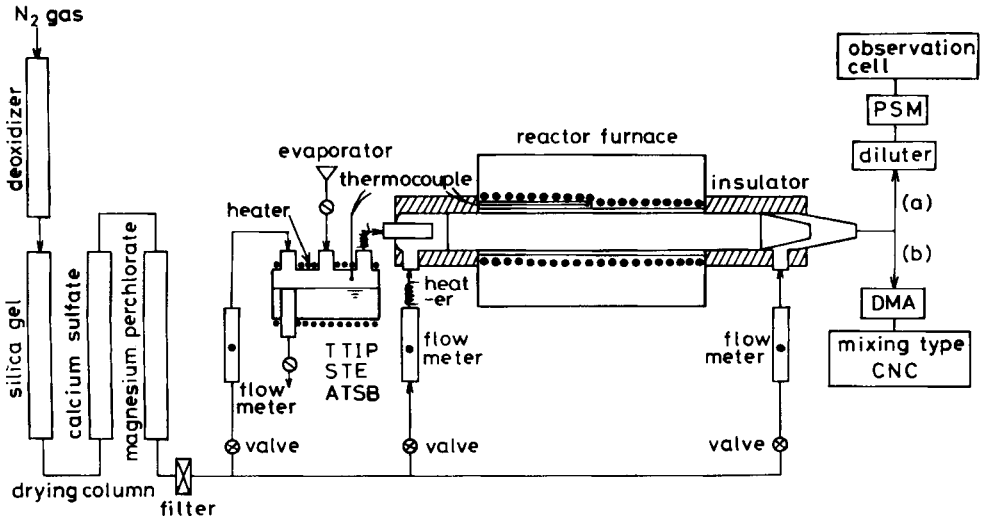

Figure 1. Experimental system for producing ultrafine metal oxide particles.

Table 1. Physical Properties of Metal Alkoxide

	$Ti(OC_3H_7)_4$	$Si(OC_2H_5)_4$	$Al(OC_4H_9)_3$
Molecular wt., g/mol	284.3	208.3	246.3
Equilib. vapor press., mm Hg	$\ln p = 21.2 - 7{,}130/T$	$\ln p = 19.3 - 5{,}555/T$	$\ln p = 23.9 - 9{,}809/T$
Density, g/cm^3	0.9555	0.935	0.967
Latent heat of vaporization, cal/g	35.21	54.9	

SI conversion: J = cal × 4.19

ultrafine aerosol from the furnace was carried out by two different methods. Particle size distributions were determined by electrostatic size analysis using a differential mobility analyzer. A portion of the aerosol was sampled and introduced into the DMA, and the number concentration of the classified aerosol was measured by means of a mixing type condensation nucleus counter (Kousaka et al., 1982). This procedure allows one to obtain the electrical mobility distribution. The particle size distributions were then determined by converting the electrical mobility distribution using Hoppel's method (Kousaka et al., 1985b) where the stationary bipolar charge distribution obtained from the bipolar charging theory of Fuchs (Adachi et al., 1985) was used. On the other hand, the remainder of the aerosol was passed through a diluter where N_2 gas was circulated in order to dilute the aerosol to about one-tenth. Then the particle number concentration of the diluted aerosol was counted independently by an ultramicroscopic system after enlarging the particles in a particle size magnifier (Okuyama et al., 1984). In the PSM, the ultrafine aerosol is continuously mixed with high-temperature air containing vapor of dibutylphathalate, which condenses on the feed aerosol to give stable droplets of about 1 μm that can be counted by an ultramicroscope. The number concentration of grown droplets was measured by observing the droplets in an observation cell using a TV camera with a He-Ne laser beam (25 mW) to illuminate individual aerosol particles.

The particles were also captured by a parallel plate electrostatic precipitator after charging with unipolar ions. Radioactive *Am*—241 was used to produce bipolar ions throughout the 4 *cm* penetration depth in air of the *Am*—241 α ray (Adachi et al., 1985). A constant electric field was applied to extract the highly mobile negative ions from the gas in order to achieve unipolar diffusion charging of the particles.

Transmission electron micrographs of aerosol particles collected under different conditions were made with an ISI Supermini scanning electron microscope (SEM) apparatus. Finally, the infrared spectra of the generated aerosols were observed with an IR spectrophotometer (Model 260-50, Hitachi Co. Ltd.) in the range 4,000 to 250 cm^{-1} at room temperature. The measurements were made on particles dispersed in KBr pellets (about 1.5 wt. %). X-ray diffraction measurements were carried out at room temperature with a Rigaku Denki Roter-frex diffractometer.

Most of experiments on thermal decomposition of alkoxide vapor were carried out using one furnace, but in some experiments a second furnace having the same inner diameter and length as the first one was added. Since temperature governs the rate of the thermal decomposition of metal alkoxide vapor and particle formation, the temperature profile was measured at the center of the furnace by a thermocouple probe. Figure 3 shows the temperature distribution for two different operating temperatures (400 and 600°C). It was found that temperatures tended to increase and decrease rather symmetrically up and down the furnace. When the second furnace, having a constant temperature of 300°C, was added, the temperature at the back part of

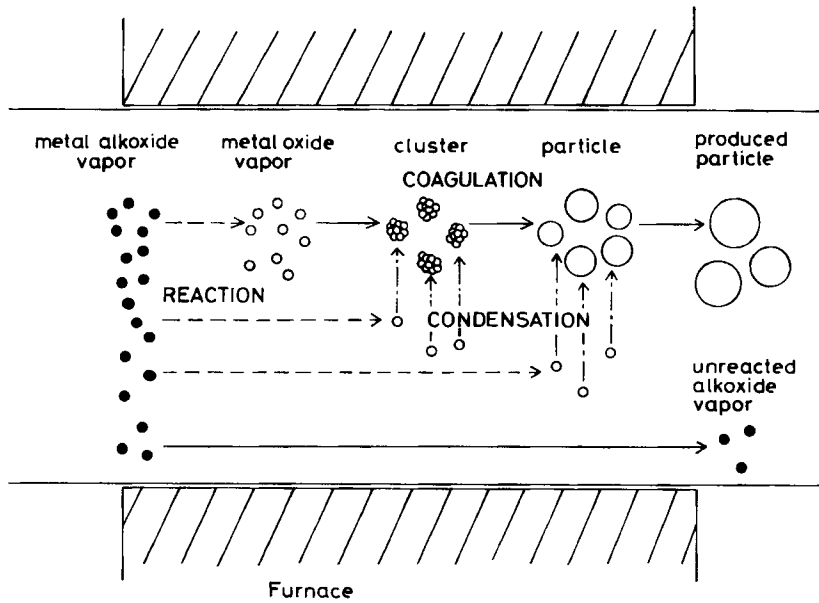

Figure 2. Particle formation in furnace.

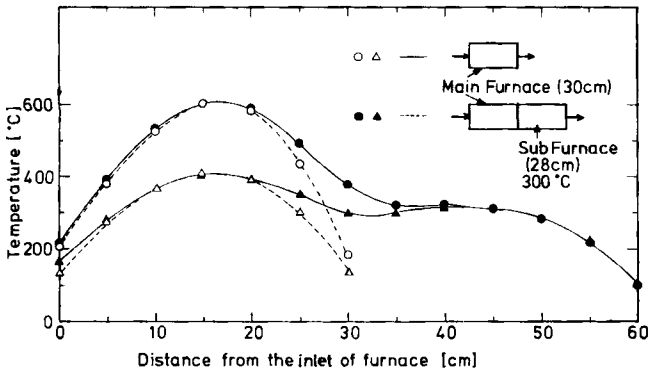

Figure 3. Temperature profile inside furnace.

the first furnace decreased less drastically. The effect of the reactor temperature distribution on the rate of particle formation was examined by adding the second furnace. It was found that there existed no significant difference between reactor temperature distributions for flow rates varying from 0.3 to 4 L/min.

Properties of Generated Particles

TiO_2 aerosol particles

Figure 4 shows the size distributions of the TiO_2 particles generated as a function of furnace temperature. In this series of experiments, the temperature of the evaporating liquid was 40°C, and the flow rate of carrier gas containing vapor was 50 cm^3/min. The nitrogen gas was added at a flow rate of 950 cm^3/min. We note that the particle size distribution of the aerosol generally is less than 100 nm (0.1 μm). Since a higher concentration of TiO_2 vapor can be obtained from thermal decomposition at a higher temperature, the particle size distribution shifts to larger sizes as the reaction temperature is increased.

Figure 5 shows the changes in size distribution of the TiO_2 aerosol due to changes in the feed vapor concentration of metal alkoxide. In this series of experiments the alkoxide vapor is produced at a temperature of 40°C, while the flow rate of vapor is varied from 50 to 100, 150, and 200 cm^3/min, and the nitrogen gas was added at 950, 900, 850, and 800 cm^3/min to maintain the total flow rate of gas in the furnace constant at 1 L/min. The temperature of the furnace was maintained at 400°C. As expected, particles grow larger as the concentration of the alkoxide vapor, C_{Ao}, is increased.

The tables with Figures 4 and 5 show the changes in geometric mean diameters d_{pg}, geometric standard deviation σ_g, and number concentration of the generated particles N_t. The values of geometric mean diameter and geometric standard deviation were obtained by plotting the experimental data on a log normal probability graph. The values Y shown in the last column indicate the percentage conversion of metal oxide vapors to aerosol. The quantity of metal oxide vapor has been calculated by assuming that the thermal decomposition is complete and that the carrier gas from the evaporator is saturated with alkoxide vapor. This quantity can be compared with the converted amount of metal oxide vapor calculated from the volume concentration of product particles and density of oxide particles. The total particle volume V was obtained by (Seinfeld, 1986),

$$V = (\pi d_v^3 N_t)/6, \qquad (2)$$

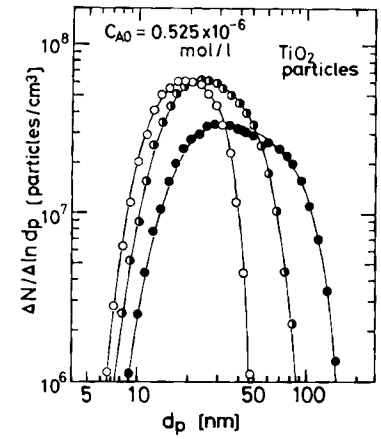

key	T_f [°C]	d_{pg}[nm]	σ_g [-]	N_t [cm^{-3}]	Y [%]
○	400	18.8	1.46	6.52x10^7	3.95
◑	500	26.0	1.62	8.08x10^7	19.5
●	600	37.2	1.88	5.68x10^7	84.1

Figure 4. Change in size distribution of TiO_2 aerosol particles with reaction temperature.

where $\ln d_v = \ln d_{pg} + 1.5 \ln^2 \sigma_g$.

As seen from the values of the yield Y, the percentage of vapor converted to aerosol varies from about 3% to over 80%, depending on the reaction conditions.

Figure 6 shows the effect of flow rate on the size distributions (geometric mean diameter and geometric standard deviation) and particle number concentrations at a constant flow rate ratio of both gases (carrier gas including the saturated vapor and gas added for the dilution) at 1:19. We see that the particles grow increasingly with decreasing total flow rate of gas in the furnace. The aerosol number concentrations and size distributions do not change until the flow rate of gas exceeds 1 L/min. Figure 7 shows how the particle size distribution and number concentration depend on the furnace length. We see that with the addition of the second furnace the total particle number concentra-

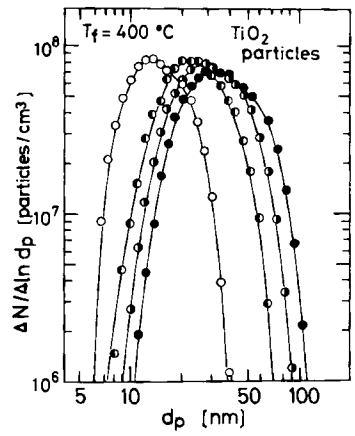

key	C_{A0}x10^6 [mol/l]	d_{pg}[nm]	σ_g [-]	N_t [cm^{-3}]	Y [%]
○	0.525	15.7	1.46	8.34 x 10^7	2.96
◐	1.05	19.1	1.49	8.85 x 10^7	3.01
◑	1.56	23.6	1.52	9.15 x 10^7	4.23
●	2.10	36.0	1.56	8.62 x 10^7	11.7

Figure 5. Change in size distribution of TiO_2 aerosol particles with TTIP vapor concentration.

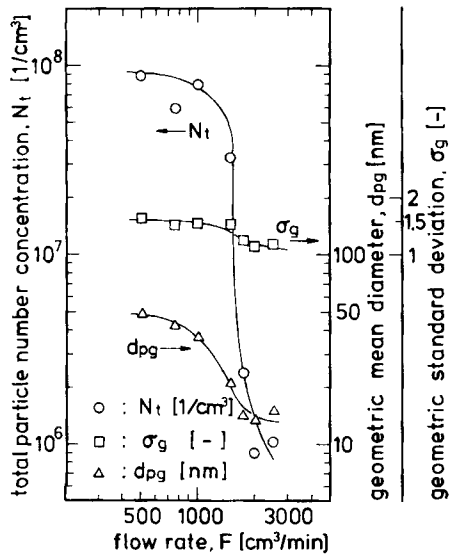

Figure 6. Effect of flow rate on particle generation.

tions and geometric standard deviations do not change, but that only the geometric mean diameters increase. The TiO_2 vapor produced by chemical reaction will deposit due to thermophoresis after the exit of furnace. The nucleation process, determining the number concentration of generated particles, is complete in the first furnace. Thus, the number concentration should not be influenced by the addition of the second furnace. However, the vapor that does not deposit on the pipe wall after the first furnace will condense on the particles generated in the first furnace, and the geometric mean diameter of the particle population will therefore increase.

The IR spectra of TiO_2 particles produced at furnace temperatures of 400, 500, and 600°C, together with the IR spectrum of the standard anatase-type TiO_2, are shown in Figure 8. Since the large absorptions between 400 and 1,000 cm^{-1} typically indicate TiO_2 as seen from the TiO_2 reference, all the produced

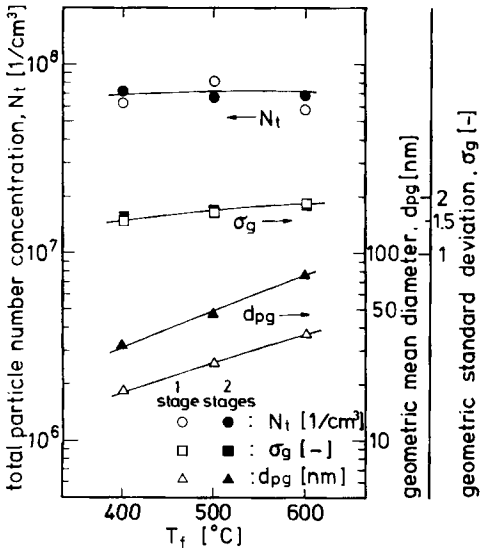

Figure 7. Effect of furnace length on particle generation.

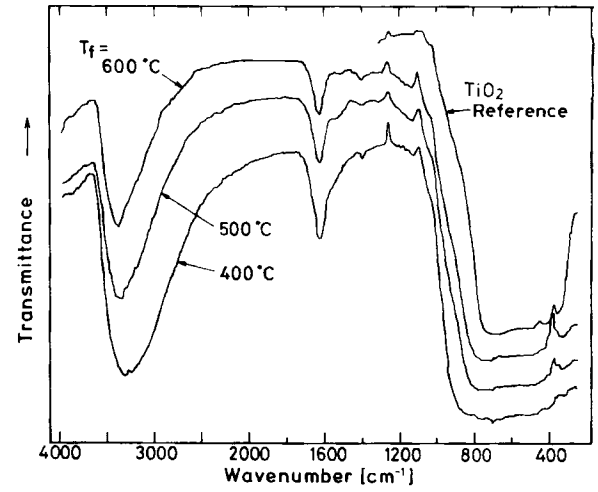

Figure 8. IR spectrum of TiO_2 particles.

particles are found to be TiO_2, irrespective of the furnace temperature. It is also seen that other absorptions at 1,630 and 3,400 cm^{-1} are due to water; their intensity tends to decrease with increasing furnace temperature. Thus, the quantity of condensed water tends to increase with the larger surface area of smaller particles that were obtained at lower furnace temperatures.

The X-ray diffraction patterns of the particles are shown in Figure 9. Compared with the standard anatase-type TiO_2, the particles produced at temperatures above 500°C are found to be anatase, whereas the particles produced at 400°C are amorphous, without the clear peaks.

SiO_2 aerosol particles

Figure 10 shows the changes in SiO_2 particle size distributions due to changes in furnace temperature. In this series of experiments the temperature of the vaporizer is 0°C, the flow

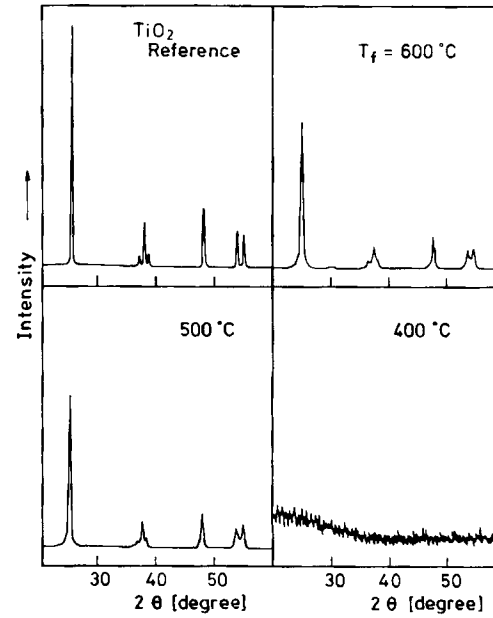

Figure 9. X-ray diffraction pattern of TiO_2 particles.

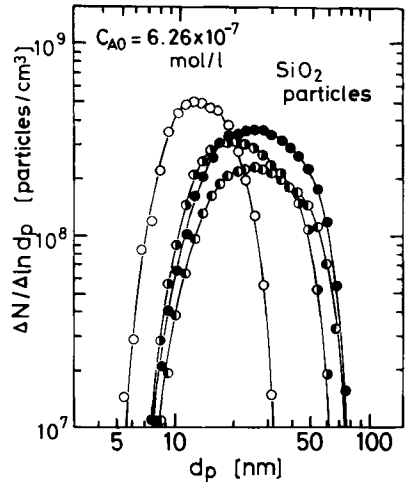

key	T_f [°C]	d_{pg} [nm]	σ_g [-]	N_t [cm^{-3}]	Y [%]
○	750	13.4	1.41	3.89×10^8	5.88
◑	800	21.5	1.57	4.32×10^8	39.7
◐	850	25.6	1.61	3.04×10^8	52.4
●	900	25.5	1.62	4.91×10^8	86.0

Figure 10. Change in size distribution of SiO_2 aerosol particles with reaction temperature.

rate of carrier N_2 gas is 30 cm^3/min, and the N_2 gas dilution flow is 970 cm^3/min. We note that the particle sizes increase with the temperature of the furnace, and the particles are all smaller than 0.1 μm. In this case, particles were not formed at temperatures lower than 700°C.

Figure 11 shows the changes in particle size distributions due to the initial concentration of STE vapor at a furnace temperature of 850°C. The experimental results show the same behavior as in the case of TiO_2 production where the size distribution of particles shift to larger sizes as the concentration of metal alkoxide vapor increases.

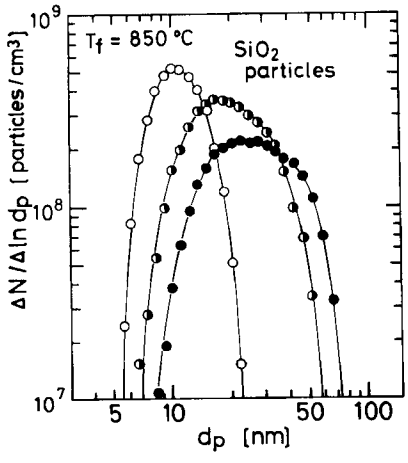

key	$C_{A0} \times 10^7$ [mol/l]	d_{pg} [nm]	σ_g [-]	N_t [cm^{-3}]	Y [%]
○	2.09	10.8	1.34	4.14×10^8	8.54
◑	4.17	19.7	1.56	4.49×10^8	46.3
●	6.26	25.6	1.61	3.04×10^8	52.4

Figure 11. Change in size distribution of SiO_2 aerosol particles with STE vapor concentration.

The particles produced were found to be SiO_2 from the IR spectra, but the particles were found to be amorphous *in all* cases.

Al_2O_3 aerosol particles

Figure 12 shows the changes in Al_2O_3 size distribution due to change in furnace temperature. In this series of experiments ATSB evaporated at 100°C was supplied at 10 cm^3/min, with the N_2 gas added at 990 cm^3/min. Although the particles are found to be smaller than 0.1 μm, the variation of the size distribution is found not to be as large as that associated with production of TiO_2 and SiO_2 particles. From the IR spectra and X-ray diffraction patterns of the produced particles, they are found to be Al_2O_3 in the amorphous state.

Electron micrographs of ultrafine particles

Figure 13 shows transmission electron micrographs of TiO_2, SiO_2, and Al_2O_3 particles dispersed on TEM mounts. The magnifications needed were 100,000–200,000X. It is seen that the primary particles range from 0.01 to 0.06 μm, and that these particles almost agree with the results measured by the differential mobility analyzer. Although there exist some agglomerated particles, we note the absence of long chain aggregates.

Simulation of Aerosol Evolution in Furnace

As shown in the diagram of the particle production process in Figure 2, particles may vary in size from vapor monomer to clusters (collections of molecules) to larger particles. The evolution of these particles occurs as a result of cluster-cluster and particle-particle collisions and individual cluster or particle growth due to accretion of vapor molecules. The vapor molecules are produced by the thermal decomposition occurring in the furnace.

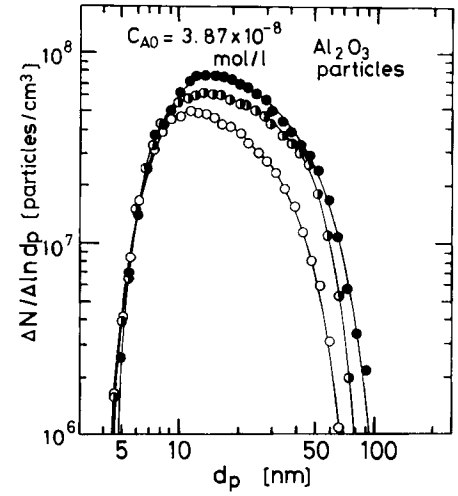

key	T_f [°C]	d_{pg} [nm]	σ_g [-]	N_t [cm^{-3}]	Y [%]
○	500	14.5	1.92	1.41×10^8	63.6
◑	700	16.9	1.95	1.06×10^8	93.6
●	900	17.8	1.99	6.82×10^7	70.2

Figure 12. Change in size distribution of Al_2O_3 aerosol particles with reaction temperature.

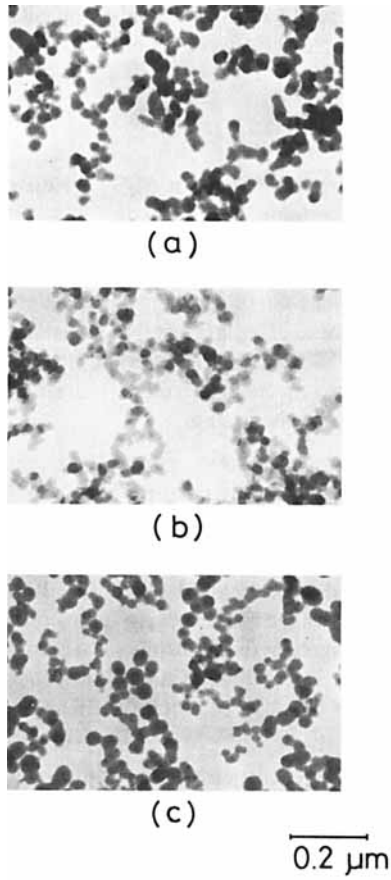

Figure 13. Transmission electron micrographs of produced ultrafine particles.

a. TiO_2 particles at reaction temperature 400°C
b. SiO_2 particles at reaction temperature 900°C
c. Al_2O_3 particles at reaction temperature 700°C

The dynamic behavior of the monomer, clusters, and particles in the gas-to-particle conversion process is described by the aerosol general dynamic equation (GDE) (Gelbard and Seinfeld, 1979; Seinfeld, 1986). Since monomer will be produced by the thermal decomposition and may exist throughout the furnace, the discrete-continuous GDE derived by Gelbard and Seinfeld is considered to be most appropriate. The interactions involving monomer, clusters, and particles is shown in Figure 14. When the number of monomers composing the particle is less than some value k, the number concentration of these clusters having i monomers is expressed by the discrete concentration, $N(v_i, t)$, whereas the number concentration of particles having monomers exceeding $2k + 1$ is characterized by volume v in the continuous expression as $n_l(v, t)d \ln v (=n(v, t)dv)$. Particles intermediate between discrete clusters and continuous particles whose monomer numbers range from $k + 1$ to $2k$ are characterized as $n(v_i, t)v_1$, where v_1 is the volume of monomer.

The balance of monomer concentration [volume is v_1 and its number concentration is $N(v_1, t)$] is

$$\frac{dN(v_1, t)}{dt} = -N(v_1, t)L(v_1, t) + S_o(v_1, t) \qquad (3)$$

For clusters [volume is v_i, $2 \le i \le k$; number concentration is $N(v_i, t)$], the basic conservation equation is

$$\frac{dN(v_i, t)}{dt} = \frac{1}{2}\sum_{j=1}^{i-1} K_B(v_i - v_j, v_j)N(v_i - v_j, t)N(v_j, t) - N(v_i, t)L(v_i, t) \qquad (4)$$

For cluster-particle intermediate particles [volume is v_i, $k + 1 \le i \le 2k$; number concentration is $n(v_i, t)v_1$], the basic conservation equation is

$$\frac{dn(v_i, t)}{dt} = \sum_{j=1}^{i-k-1} K_B(v_i - v_j, v_j)N(v_j, t)n(v_i - v_j, t) \quad i \ge k + 2$$
$$+ \frac{1}{2}\sum_{j=i-k}^{k} K_B(v_i - v_j, v_j)\, N(v_i - v_j, t)N(v_j, t)/v_1 - n(v_i, t)L(v_i, t) \qquad (5)$$

For continuous particles [volume is $v(>v_{2k} + v_1/2)$; number concentration is $n_l(v, t)d \ln v$], the basic equations are

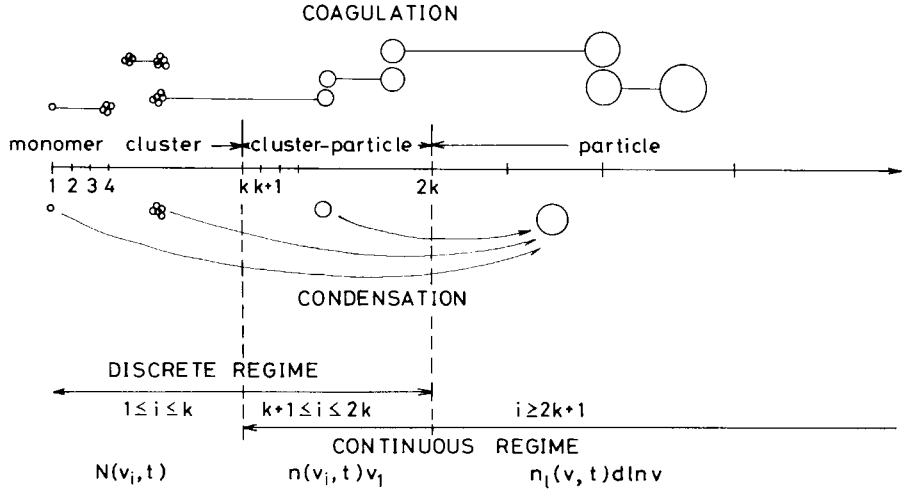

Figure 14. Representation of monomer, clusters, and particles used in discrete-continuous general dynamic equation.

$$\frac{\partial n_l(v,t)}{\partial t} = v\sum_{j=1}^{k} K_B(v-v_j, v_j)N(v_j,t)\frac{n_l(v-v_j,t)}{v-v_j}$$

$$+\begin{cases}\dfrac{1}{2}v\displaystyle\int_{v_{k+1}-v_1/2}^{v-v_{k+1}-v_1/2} K_B(v-u,u)\times\frac{n_l(v-u,t)}{v-u}n(u,t)\,du, \\ \quad v-v_{k+1}+v_1/2 \le v_{2k}+v_1/2 \\ \dfrac{1}{2}v\displaystyle\int_{v_{k+1}-v_1/2}^{v_{2k}+v_1/2} K_B(v-u,u)\times\frac{n_l(v-u,t)}{v-u}n(u,t)\,du \\ \quad +\dfrac{1}{2}v\displaystyle\int_{v_{2k}+v_1/2}^{v-v_{k+1}+v_1/2} K_B(v-u,u)\frac{n_l(v-u,t)}{v-u}n_l(u,t)\,d\ln u, \\ \quad v-v_{k+1}+v_1/2 > v_{2k}+v_1/2\end{cases}$$

$$-n_l(v,t)L(v,t) \qquad (6)$$

Here, $L(v',t)$ can given by

$$L(v',t) = \sum_{j=1}^{k} K_B(v',v_j)N(v_j,t) + \int_{v_{k+1}-v_1/2}^{v_{2k}+v_1/2} K_B(v',u) \times n(u,t)\,du + \int_{v_{2k}+v_1/2}^{\infty} K_B(v',u)n_l(u,t)\,d\ln u \qquad (7)$$

In Eq. 3, $S_o(v_1,t)$ is the generation rate of monomer by the chemical reaction. When the thermal decomposition of metal alkoxide vapor in the furnace is assumed to be expressed as a first-order reaction, the chemical reaction rate can be given by

$$r_p = dC_p/dt = -dC_A/dt = k_A C_A \qquad (8)$$

where C_p is the concentration of metal oxide monomer, C_A is the monomer concentration of metal alkoxide vapor, and k_A is the reaction rate constant. Accordingly, $S_o(v_1,t)$ can be given by

$$S_o(v_1,t) = r_p M_p/(\rho_p v_1) = (k_A C_{Ao} e^{-k_A t})M_p/(\rho_p v_1) \qquad (9)$$

where C_{Ao} is the concentration of alkoxide vapor supplied to the furnace and M_p is the molecular weight of metal oxide particles.

In the derivation of Eqs. 3–7 the following assumptions are made:

1. The velocity profile of gas in the furnace is flat, and the residence time t corresponds to z/u_{av}, where z is the length from the inlet of the furnace and u_{av} is the average flow rate of gas.
2. Particles are spherical and electrically neutral.
3. Particles collide with each other to form single new spherical particle whose mass is the same as the combined mass of two smaller particles.
4. Particle deposition onto the furnace and pipe walls is negligible.
5. Evaporation of monomer from clusters or particles can be ignored because of the very low values of saturated vapor pressure and surface tension.

For the Brownian coagulation coefficient of spherical particles with volumes v and v', $K_B(v,v')$, the Fuchs (1964) interpolation formula, which expresses the coagulation rate function for the whole range of Knudsen numbers, was used (Seinfeld, 1986). The effect of van der Waals forces on the coagulation rate was not included. Since the evaluation of van der Waals forces for metal oxide particles is not available, this effect was not considered in simulating the data.

Since the discrete-continuous GDE cannot be solved analytically, the following numerical approximation method is employed. In this equation, the value of k is given as 25 and the maximum size of particles is 0.2 μm. The particle volume range, from particles having $2k+1$ monomers to the largest particle of 0.2 μm, is divided into 50 segments on a logarithmic scale. The set of simultaneous ordinary differential equations resulting are integrated by the Runge-Kutta-Merson method. The integrals in the equations are evaluated by the 40-point Guassian-Legendre quadrature formula. As a check of the accuracy of the numerical solution, the total volume of the aerosol was calculated under coagulation-predominant conditions and its difference from the inlet value was found to be within 5%.

Figures 15–17 respectively show comparisons of the predicted particle size distributions with the experimental results for TiO_2, SiO_2, and Al_2O_3 particles. In the conditions of this case, the metal alkoxide vapor supplied to the furnace is almost completely converted to metal oxide vapor, as seen from the value of yield Y being about 100% from the tables below Figs. 4, 10, and 12. Accordingly, the initial concentration of the metal alkoxide vapor supplied to the furnace C_{Ao} was calculated from the vapor pressure. In Figure 15, the broken-line curves were obtained by

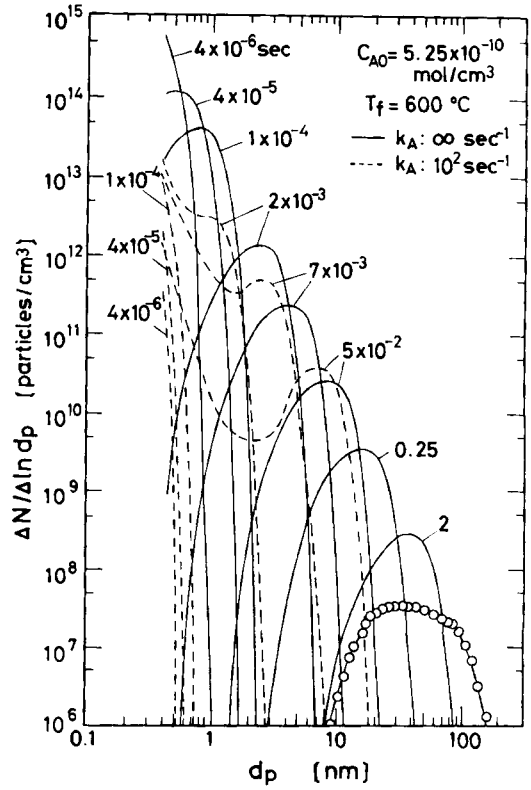

Figure 15. Comparison of calculated and experimental size distribution of produced TiO_2 particles.

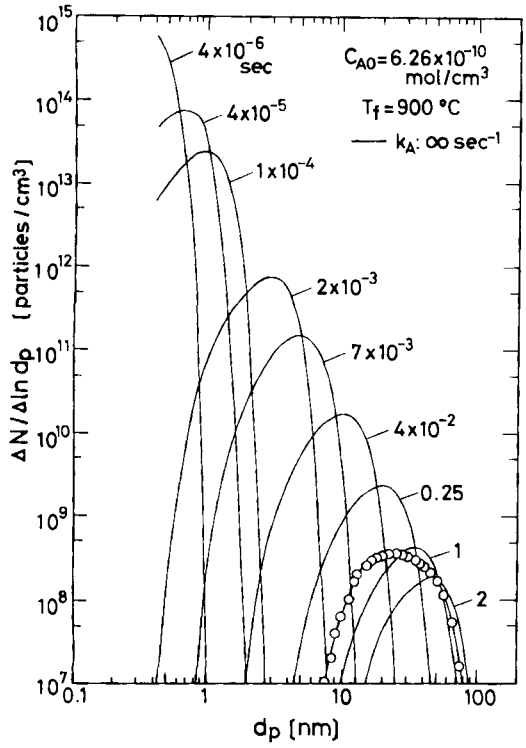

Figure 16. Comparison of calculated and experimental size distribution of produced SiO_2 particles.

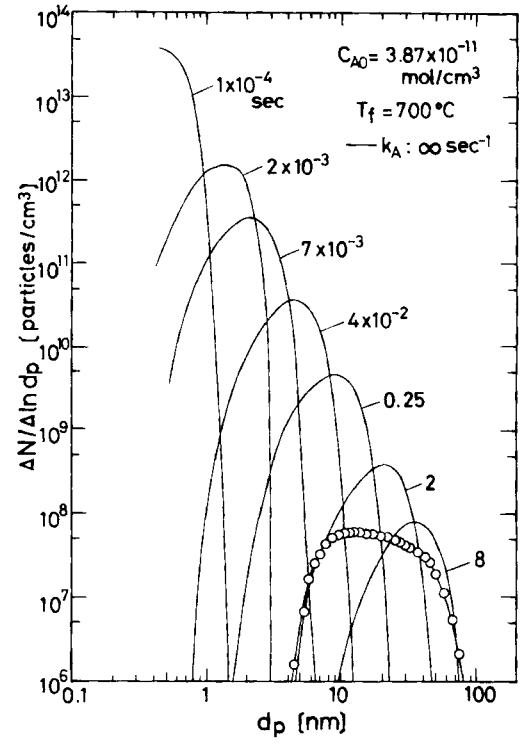

Figure 17. Comparison of calculated and experimental size distribution of produced Al_2O_3 particles.

assuming the first-order thermal decomposition rate constant k_A to be 10^2 s^{-1}, and the solid curves were obtained by assuming that the thermal decomposition is sufficiently rapid to terminate the thermal decomposition at the inlet of the furnace. In the case when the rate constant k_A is 10^2 s^{-1}, the thermal decomposition ceases within about 0.2 s. As seen from both calculation results, there exists a large difference in the change of particle size distribution until the thermal decomposition is terminated. After a sufficient lapse of time, both changes in size distribution are found to agree well with each other. It is seen that the measured size distributions agree reasonably well with those predicted for the actual residence time of 2 s. This essential agreement indicates that coagulation is the fundamental phenomenon determining particle formation by the thermal decomposition of metal alkoxide vapor. In other experimental conditions where the value of yield is much less than 100% (thermal decomposition of metal alkoxide vapor was not terminated), detailed comparison is not been possible because the reaction rate of vapor has not been well studied.

Conclusion

The production of ultrafine titanium, silicon, and aluminium oxide particles has been studied experimentally by the thermal decomposition of metal alkoxide vapor in a furnace, and the following conclusions are obtained.

1. Ultrafine TiO_2, SiO_2, and Al_2O_3 particles having geometric mean diameters ranging between 0.01 and 0.06 μm and geometric standard deviation of around 1.4 can be obtained, and particle size distributions can be controlled by the feed concentration of metal alkoxide vapor and the reactor furnace temperature.

2. Particles generated are amorphous at furnace temperatures lower than 400°C for TiO_2 particles, and 1,000°C for SiO_2 and Al_2O_3 particles.

3. Under conditions where the thermal decomposition of metal alkoxide vapors ceases in an early stage, the measured particle size distributions from the reactor furnace can be qualitatively explained by numerical solution of the discrete-continuous general dynamic equation and indicate that coagulation is the dominant process.

Acknowledgment

This work was supported by Japan Grant in Aid for Scientific Research No. 60750876, Japan Grant in Aid for Environmental Science No. 60030039, and National Science Foundation Grant No. ATM-8503103.

Notation

C_A = monomer concentration of metal alkoxide vapor, mol/cm^3
C_{Ao} = concentration of alkoxide vapor into furnace, mol/cm^3
C_P = concentration of produced metal oxide monomer, mol/cm^3
d_p = particle diameter, cm, μm, nm
d_{pg} = geometric mean diameter, cm, nm
d_v = mean volume diameter, cm, nm
F = volume flow rate of gas, cm^3/min
i = number of monomer
$K_B(v, v')$ = Brownian coagulation rate function for two particles of volume V and V', cm^3/s
k = maximum monomer number of clusters
k_A = reaction rate constant, s^{-1}
$L(V', t)$ = defined in Eq. 7
M_P = molecular weight of particle, g/mol
N_t = total particle number concentration, particles/cm^3

$N(v_i, t)$ = number concentration of clusters, particles/cm^3
$n(v_i, t)v_1$ = number concentration of cluster-particles, intermediate particles, particles/cm^3
$n_1(v, t)d \ln v$ = number concentration of particles, particles/cm^3
p = equilibrium vapor pressure of metal alkoxide, mm Hg
r_P = chemical reaction rate, mol/cm^3 · s
$S_o(v_1, t)$ = generation rate of monomer by chemical reaction, particles/cm^3 · s
T = absolute temperature, K
T_f = temperature of furnace, °C
t = time, s
u_{av} = Average flow rate of gas, cm/sec
V = total particle volume concentration, cm^3/cm^3
v = particle volume, cm^3
v_i = particle volume having i monomers, cm^3
Y = concentration ratio of supplied metal oxide vapor to produced particles, %
z = length from inlet of furnace, cm
$\Delta N/\Delta \ln d_p$ = particle size distribution function, particles/cm^3
θ = diffraction angle, degrees
ρ_P = particle density, g/cm^3
σ_g = geometric standard deviation

Literature cited

Adachi, M., Y. Kousaka, and K. Okuyama, "Unipolar and Bipolar Diffusion Charging of Ultrafine Aerosol Particles," *J. Aerosol Sci.*, **16,** 109 (1985).

Fuchs, N. A., *The Mechanics of Aerosols*, Pergamon, Oxford (1964).

Gelbard, F., and J. H. Seinfeld, "The General Dynamic Equation for Aerosols: Theory and Application to Aerosol Formation and Growth," *J. Colloid Interface Sci.*, **68,** 363 (1979).

Ingerbrethesen, B. J., and E. Matijevic, "Preparation of Uniform Colloidal Dispersions by Chemical Reactions in Aerosols. II: Spherical Particles of Aluminium Hydrous Oxide," *J. Aerosol Sci.*, **11,** 271 (1980).

Ingerbrethesen, B. J., E. Matijevic, and R. E. Partch, "Preparation of Uniform Colloidal Dispersions by Chemical Reactions in Aerosols. III: Mixed Titania/Alumina Colloidal Spheres," *J. Colloid Interface Sci.*, **95,** 228 (1983).

Kanai, T., H. Komiyama, and H. Inoue, "TiO_2 Particles by Chemical Vapor Deposition—Particle Formation Mechanism and Chemical Kinetics," ***Kagaku Kogaku Ronbunshu,*** **11,** 317 (1985).

Komiyama, H., T. Kanai, and H. Inoue, "Preparation of Porous, Amorphous, and Ultrafine TiO_2 Particles by Chemical Vapor Deposition," *Chem. Let.*, 1283 (1984).

Kousaka, Y., T. Niida, K. Okuyama, and H. Tanaka, "Development of a Mixing Type Condensation Nucleus Counter," *J. Aerosol Sci.*, **12,** 231 (1982).

Kousaka, Y., K. Okuyama, and M. Adachi, "Determination of Particle Size Distribution of Ultrafine Aerosols Using Differential Mobility Analyzer," *Aerosol Sci. Technol.*, **4,** 209 (1985a).

Kousaka, Y., K. Okuyama, T. Niida, T. Hosokawa, and T. Mimura, "Activation of Ultrafine Particles by Supersaturation in Condensational Process," *Particle Characterization,* **2,** 119 (1985b).

Okuyama, K., Y. Kousaka, and T. Motouchi, "Condensational Growth of Ultrafine Aerosol Particles in New Particle Size Magnifier," *Aerosol Sci. Technol.*, **3,** 353 (1984).

Seinfeld, J. H., *Atmospheric Chemistry and Physics of Air Pollution,* Wiley-Interscience, New York (1986).

Vica, M., and E. Matijevic., "Preparation of Uniform Colloidal Dispersions by Chemical Reactions in Aerosols. I: Spherical Particles of Titanium Dioxide," *J. Colloid Interface Sci.*, **68,** 308 (1979).

Manuscript received Mar. 17, 1986.